A Multimodal Genotoxic Anticancer Drug Characterized by Pharmacogenetic Analysis in *Caenorhabditis elegans*

Frank B. Ye,* Akil Hamza,* Tejomayee Singh,* Stephane Flibotte,† Philip Hieter,*,[1] and Nigel J. O'Neil*,[1]
*Michael Smith Laboratories and †Department of Zoology, University of British Columbia, Vancouver, V6T 1Z4, Canada
ORCID IDs: 0000-0001-9908-0626 (F.B.Y.); 0000-0002-3613-8744 (A.H.); 0000-0002-6477-1280 (T.S.); 0000-0003-3116-7017 (P.H.); 0000-0002-1992-6976 (N.J.O.)

ABSTRACT New anticancer therapeutics require extensive *in vivo* characterization to identify endogenous and exogenous factors affecting efficacy, to measure toxicity and mutagenicity, and to determine genotypes that result in therapeutic sensitivity or resistance. We used *Caenorhabditis elegans* as a platform with which to characterize properties of the anticancer therapeutic CX-5461. To understand the processes that respond to CX-5461-induced damage, we generated pharmacogenetic profiles for a panel of *C. elegans* DNA replication and repair mutants with common DNA-damaging agents for comparison with the profile of CX-5461. We found that multiple repair pathways, including homology-directed repair, microhomology-mediated end joining, nucleotide excision repair, and translesion synthesis, were needed for CX-5461 tolerance. To determine the frequency and spectrum of CX-5461-induced mutations, we used a genetic balancer to capture CX-5461-induced mutations. We found that CX-5461 is mutagenic, resulting in both large copy number variations and a high frequency of single-nucleotide variations (SNVs), which are consistent with the pharmacogenetic profile for CX-5461. Whole-genome sequencing of CX-5461-exposed animals found that CX-5461-induced SNVs exhibited a distinct mutational signature. We also phenocopied the CX-5461 photoreactivity observed in clinical trials and demonstrated that CX-5461 generates reactive oxygen species when exposed to UVA radiation. Together, the data from *C. elegans* demonstrate that CX-5461 is a multimodal DNA-damaging anticancer agent.

KEYWORDS *Caenorhabditis elegans*; pharmacogenetics; G-quadruplex; DNA repair; chemotherapeutic

KEY to the adoption of targeted anticancer therapies is an understanding of the interactions between therapeutic agents, tumor genotypes, and tumor environments. The properties of therapeutic candidates need to be assayed to determine: (1) their mechanisms of action, (2) mutagenicity, and (3) pharmacogenetic profiles, which are the effects of genotypes on therapeutic sensitivity and resistance. Genotype is a major determinant of chemotherapeutic toxicity and efficacy. Screening for therapeutic-sensitive and -resistant genotypes can identify tumor-specific genetic biomarkers and contribute to the understanding of the mechanism of action of anticancer therapeutics. Many pharmacogenomic screens have been conducted in human cell lines using RNA interference or, more recently, clustered regularly interspaced short palindromic repeats single guide RNA libraries, to identify anticancer pharmacogenetic interactions (Jiang *et al.* 2011; Barretina *et al.* 2012; Garnett *et al.* 2012; Basu *et al.* 2013; Iorio *et al.* 2016; Srivas *et al.* 2016). While cell lines can be useful, the genotypes of many cell lines are not well characterized and can evolve because of genomic instability. A more genetically stable, near isogenic assay system could be utilized to take a more reductive approach to determine pharmacogenetic interactions with new potential therapeutics.

The nematode *Caenorhabditis elegans* is an attractive animal model with which to characterize the properties of anticancer therapeutics. The small size, ease of handling, and powerful genetic tools of *C. elegans* provide a sophisticated

doi: https://doi.org/10.1534/genetics.120.303169
Manuscript received March 11, 2020; accepted for publication May 8, 2020; published Early Online May 15, 2020.
Available freely online through the author-supported open access option.
Supplemental material available at figshare: https://doi.org/10.25386/genetics.12307637.
[1]Corresponding authors: Rm 323, Michael Smith Laboratories, University of British Columbia, 2185 East Mall, Vancouver, BC, Canada V6T 1Z4. E-mail addresses: hieter@msl.ubc.ca; and noneil@msl.ubc.ca

in vivo platform that combines the technical advantages of a microorganism with the greater biological complexity of a multicellular organism. *C. elegans* has been used to screen for and characterize compounds affecting meiosis (Allard *et al.* 2013; Shin *et al.* 2019) and development (Harlow *et al.* 2016). *C. elegans* has also proven useful for determining mutational frequencies and signatures of DNA damage response mutants and genotoxic agents (Rosenbluth *et al.* 1983, 1985; Zhao *et al.* 2008; Meier *et al.* 2014; van Schendel *et al.* 2016).

CX-5461 is a promising anticancer therapeutic candidate currently in clinical trials (Hilton *et al.* 2018; Khot *et al.* 2019). CX-5461 was first described as an orally bioavailable RNA polymerase (RNA Pol) I inhibitor that exhibited antitumor activity in murine xenograft models (Drygin *et al.* 2011) and was the first RNA Pol I inhibitor to be tested in clinical trials (Khot *et al.* 2019). CX-5461 activity is not limited to RNA Pol I inhibition. CX-5461 has also been shown to stimulate ATM/ATR activation (Negi and Brown 2015), and rapamycin-associated signaling (Li *et al.* 2016). More recently, it was found that homology-directed repair (HDR)-deficient cancer cell lines are sensitive to CX-5461 and that this sensitivity may be due to the stabilization of G-quadruplex (G4)-forming DNA structures that could affect DNA replication (Xu *et al.* 2017). This has led to a clinical trial focusing on patients with HDR-deficient tumors (Hilton *et al.* 2018). However, the mechanisms underlying the tumor cell-killing and *in vivo* properties of CX-5461 are still unclear.

We used *C. elegans* to assay CX-5461-mediated photosensitivity, mutagenicity, and mutational signatures, and identified genotypes that are sensitive to CX-5461. We found that CX-5461 is a multimodal genotoxic agent with similarities to the antineoplastic ellipticine- and anthracycline-based anticancer agents. A better understanding of the properties of CX-5461 will assist the development of this promising anticancer therapeutic candidate.

Materials and Methods

Strains and culturing

Nematode strains were maintained as described previously (Brenner 1974). The alleles used in this study were: *atm-1(tm5027)*, *brd-1(dw1)*, *rfs-1(ok1372)*, *cku-80(ok861)*, *lig-4(ok716)*, *hsr-9(ok759)*, *polq-1(tm2026)*, *polh-1(lf31)*, *polk-1(lf29)*, *fcd-2 (tm1298)*, *fan-1(tm423)*, *fncm-1(tm3148)*, *msh-2(ok2410)*, *ercc-1(tm1981)*, *xpa-1(ok698)*, *mus-81(tm1937)*, *rcq-5(tm424)*, *rtel-1(tm1866)*, *helq-1 (tm2134)*, *dog-1(gk10)*, *wrn-1(gk99)*, *let-418(n3536)*, *him-1(e879)*, *hda-3(ok1991)*, *gld-1(op236)*, *cep-1(gk138)*, *dvc-1(ok260)*, *smrc-1(gk176502)*, and *polz-1/rev-3(gk919715)*. Bristol N2 was used as wild-type in all experiments. Some strains were provided by the *Caenorhabditis* Genetics Center, which is funded by National Institutes of Health Office of Research Infrastructure Programs (P40 OD-010440), and some knockout alleles were provided by the Shohei Mitani laboratory. *smrc-1(gk176502)*, *smrc-1(gk784642)*, and *polz-1/rev-3(gk919715)* were Million Mutation Project alleles (Thompson *et al.* 2013) provided by the Moerman laboratory, and were outcrossed at least six times. Some strains were generated by the International *C. elegans* Gene Knockout Consortium (*C. elegans* Deletion Mutant Consortium, 2012) and by the National Bioresource Project of Japan.

UVA irradiation

UVA source: predominantly 365 nm, from a Black-RayUV Bench Lamp (model: XX-15L). Before each UVA exposure, the light source output was determined by a long-wave UV measuring meter (model: J-221). Different UVA exposures were achieved by varying the exposure times.

Quantitative acute assay

For CX-5461 assays, synchronized 1-day-old adults were incubated in CX-5461 (in NaH_2PO_4) or NaH_2PO_4 diluted in M9 buffer containing *E. coli* OP50, carbenicillin (50 μg/ml), and 1× nystatin for ∼18 hr. For etoposide (ETP) and camptothecin (CPT), synchronized 1-day-old adults were incubated in agents (100 nM CPT or 100 μM ETP) or DMSO solvent diluted in M9 buffer containing OP50, carbenicillin (50 μg/ml), and 1× nystatin for ∼18 hr.

Following treatment, the animals were allowed to recover for 0.5 hr on OP50-containing NGM plates before UVA irradiation (if applicable), then plated at 10 per plate in triplicate on NGM plates for a 4-hr interval (18–22 hr post-treatment), and then removed. The numbers of both arrested embryos and hatching larvae were counted 1 day later to calculate the percentage of embryo survival after treatment. All results were from at least 30 treated animals (three plates with 10 animals per plate). The sensitivity score was calculated by normalizing the embryo survival rate under drug-treated conditions to the nondrug condition with respect to that of wild-type N2 animals.

Quantitative acute assay for UVA-trimethylpsoralen

Synchronized 1-day-old adults were washed off plates and resuspended in 10 μg/ml trimethylpsoralen (TMP) diluted in 500 μl M9 buffer containing 0.1% Triton X for 1 hr in the dark. Following treatment, the animals were washed in M9 buffer and then transferred to two OP50-containing NGM plates. Next, one plate was exposed to UVA irradiation. Both plates were kept in the dark to avoid UVA from light in the laboratory. Ten worms were transferred in triplicate to NGM plates for a 3-hr interval and then removed. The numbers of arrested embryos and hatching larvae were counted 1 day later to calculate the percentage of embryo survival after treatment. The sensitivity score was calculated by normalizing the embryo survival rate under UVA-exposed conditions to non-UVA conditions with respect to that of wild-type N2 animals.

Quantitative acute assay for UVC

Synchronized 1-day-old adults were exposed to UVC irradiation (or mock treatment). The UVC source was provided by a

UV cross-linker (spectrolinker XL-1000, Spectronics Corporation) with 254-nm bulbs (spectrolinker). Animals were kept in the dark overnight. Ten worms were transferred in triplicate to NGM plates for a 2.5-hr interval (18–21 hr postirradiation) and then removed. The numbers of arrested embryos and hatching larvae were counted 1 day later to calculate the percentage of embryo survival after treatment. The sensitivity score was calculated by normalizing the embryo survival rate under UVC-irradiated conditions to non-UVC conditions with respect to that of wild-type N2 animals.

Mutagenesis screen for CX-5461

Strain BC2200 *dpy-18/eT1(III);unc-46/eT1(V)* was used in the mutagenesis screen. *dpy-18/eT1(III);unc-46/eT1(V)* animals were treated with or without 100 μM CX-5461 for 18 hr before UVA irradiation, and 200 single *dpy-18/eT1(III);unc-46/eT1(V)* F1s were picked in each condition. A sterile phenotype at F1 was considered to have acquired a dominant lethal mutation, and lines in which the F2 or later generations did not have Dpy Unc animals were counted as acquiring recessive lethal mutations on balanced regions of chromosome III or V.

Genome sequencing

The lines that acquired recessive lethal mutations were maintained for at least three generations. Worms were rinsed off with deionized water and concentrated. Genomic DNA was purified using Puregene Core Kit A (QIAGEN, Valencia, CA). DNA sequencing was performed at the Novogene Bioinformatics Institute (Beijing, China). Sequence reads were mapped to the *C. elegans* reference genome version WS230 (http://www.wormbase.org) using the short-read aligner BWA (Li and Durbin 2010), which resulted in an average sequencing depth for each sample ranging from 22× to 57× with a median of 34×. Single-nucleotide variations (SNVs) and small insertions/deletions were identified and filtered with the help of the SAMtools toolbox (Li *et al.* 2009). Candidate variants at genomic locations for which the parental N2 strain had an agreement rate with the reference genome < 95% were eliminated from further consideration. Each variant was annotated with a custom Perl script and gene information downloaded from WormBase version WS230. Copy numbers were estimated from the alignments with a procedure analogous to that of Itani *et al.* (2016) using 5-kb wide overlapping sliding windows with the alignments from the parental strain used as the reference.

CX-5461 agarose gel shift and mung bean endonuclease assays

To test whether CX-5461 could intercalate into DNA, we incubated CX-5461 for 1 hr at room temperature with a PCR-generated double-stranded DNA (dsDNA) fragment and visualized the migration of DNA on a 1% agarose gel containing the dsDNA-specific dye SYBR-Safe. PCR products (~40 ng/μl) were mixed with CX-5461 at room temperature. The CX-5461-DNA mixtures were incubated at 94° for 25 min to denature the dsDNA, and then the temperature was monitored and decreased stepwise until the target temperature was reached. For the nuclease cleavage experiment, 10,000 U/ml mung bean nuclease (MBN) (catalog number M0250S; New England BioLabs, Beverly, MA) was added to the CX-5461-DNA mixtures at room temperature (1.75 μl MBN per 100 μl reaction). Then, the mixture was incubated for 1 hr at either 25° or 40°. The final CX-5461-DNA products were loaded onto a 1% agarose gel containing SYBR-Safe DNA stain for visualization. To determine whether CX-5461 affected mung bean endonuclease activity, we incubated a PCR product predicted to form a G4 and a PCR product without a predicted G4 (non-G4) with MBN, which cleaves single-stranded or distorted dsDNA, for 1 hr at the specified temperatures and assessed the endonuclease activity on a 1% Syber-Safe-containing agarose gel.

L1 exposure assay

Gravid animals were synchronized in the L1 stage by hypochlorite treatment (0.5 M NaOH and 2% hypochlorite). After overnight starvation, ~100 L1 larvae of each mutant strain were incubated in 50 μl of M9 buffer containing OP50, carbenicillin (50 μg/ml), 1× nystatin, and 500 μM NaH_2PO_4 with and without 100 μM CX-5461 for ~18 hr. Following treatment, worms were allowed to recover for 0.5 hr on OP50-containing NGM plates before they were irradiated with the indicated amount of UVA exposure. Animals were imaged 4 days following UVA exposure at 20X magnification using a Thermo Fisher Scientific EVOS microscope.

Reactive oxygen species measurement with 2′,7′-dichlorodihydrofluorescein diacetate

Adult worms treated in 100 μM CX-5461 for 18 hr were added with 25 μM 2',7'-dichlorodihydrofluorescein diacetate (H_2DCFDA), and incubated for another hour in the dark before initial fluorescence measurement using a microplate reader. After initial measurement, worms were irradiated with the indicated amount of UVA exposure and then immediately sent for a second measurement (Yoon *et al.* 2017).

Generational survival assay

Animals were plated individually and maintained at room temperature. Starting with 20 separate lines at the P_0 generation, a single L4-stage animal was transferred to a fresh plate at each generation. A line was scored as unsustainable when the parent worm was either sterile or produced only dead embryos.

Cell culture and treatment with CX-5461

HCT116 and HT29 wild-type cells were obtained from the American Type Culture Collection. Cells were cultured in McCoy's 5A medium (Life Technologies) supplemented with 10% FBS at 37° and 5% CO_2. CX-5461 was purchased from Selleck Chemicals. Cells were seeded in a 96-well format (six technical replicates) and after 24 hr, CX-5461 (or DMSO) diluted in McCoy's 5A medium was added to the wells.

Two hours postincubation in the drug, cells were exposed to 50 J/m^2 UVA and allowed to grow for 4–5 days. Cells were fixed in 3.7% paraformaldehyde and stained with Hoechst 33342 before nuclei were counted on a Cellomics Arrayscan VTI.

Yeast assays

Wild-type (BY4742) and *rad52*Δ yeast strains were diluted from midlog phase to OD_{600} = 0.01 in 200 μl SC media ± CX-5461 in 96-well plates. Cells were incubated for 3 hr ± CX-5461 with constant shaking before UVA treatment and subsequent loading to a TECAN M200 plate reader. OD_{600} readings were measured every 30 min over a period of 24 hr and plates were shaken for 10 min before each reading. Strains were tested in three replicates per plate per condition and the area under the curve (AUC) was calculated for each replicate. Strain fitness was defined as the AUC of each yeast strain relative to the AUC of the wild-type strain (without CX-5461 and UVA treatment) grown on the same plate.

Data availability

The raw sequence data from this study have been submitted to the National Center for Biotechnology Information BioProject (http://www.ncbi.nlm.nih.gov/bioproject) under accession number PRJNA540967 and can be accessed from the Sequence Read Archive (https://www.ncbi.nlm.nih.gov/sra). Supplemental material available at figshare: https://doi.org/10.25386/genetics.12307637.

Results

Pharmacogenetic profile of CX-5461

To characterize the DNA damage response to CX-5461, we generated pharmacogenetic profiles for four common DNA-damaging agents [the topoisomerase I poison CPT; the topoisomerase II poison ETP; the interstrand cross-linking (ICL) agent UVA-activated TMP (UVA-TMP); and UVC radiation (UVC), which causes thymine dimers and photoproducts] and CX-5461, using a panel of 28 *C. elegans* DNA replication and repair mutants that represented the major DNA damage response pathways. A range of DNA-damaging agent concentrations were tested and the final concentration was selected to maximize the effect in sensitive mutants while minimizing the effect on wild-type animals.

The pharmacogenetic profile of CX-5461 demonstrates that multiple DNA damage response pathways are required for CX-5461 tolerance. Sensitivity to CX-5461 was observed in 14 of the 28 DNA damage response mutants tested (Table 1). The CX-5461 pharmacogenetic profile was distinct from the other DNA-damaging agents, sharing some but not all genotypic sensitivities. Of the 14 CX-5461-sensitive strains, 13 were sensitive to UVA-TMP, 9 were sensitive to UVC, 8 were sensitive to CPT, and 10 were sensitive to ETP. Although there were overlapping genotypic sensitivities of CX-5461 and UVA-TMP, Fanconi anemia pathway mutants were not sensitive to CX-5461, which demonstrated that CX-5461 does not result in ICLs. The CX-5461 pharmacogenetic profile was also similar to that of the topoisomerase poisons CPT and ETP (Figure 1A). The major difference was that translesion synthesis (TLS) and nucleotide excision repair (NER) mutants were exquisitely sensitive to CX-5461 and not to either topoisomerase poison, which differentiated the CX-5461 profile from those of the topoisomerase poisons.

HDR and microhomology-mediated end joining are required for CX-5461 tolerance

Mutations affecting double-strand break (DSB) repair pathways caused differential sensitivity to topoisomerase poisons and CX-5461. Nonhomologous end joining mutants were not sensitive to topoisomerase poisons or CX-5461. HDR mutants (*brd-1*, *rfs-1*, and *helq-1)* were very sensitive to CPT but only mildly sensitive to ETP, whereas the microhomology-mediated end-joining (MMEJ) mutant *polq-1* was very sensitive to ETP but not sensitive to CPT. In contrast, mutations affecting either HDR or MMEJ resulted in moderate sensitivity to CX-5461. To test whether HDR and MMEJ were contributing independently to the repair of CX-5461-induced lesions, we tested *polq-1 brd-1*, *rfs-1 polq-1*, and *helq-1 polq-1* double mutants for increased sensitivity to CX-5461. In all three cases, the double mutants exhibited increased CX-5461 sensitivity suggesting that HDR and MMEJ contributed independently to the repair of CX-5461-induced lesions (Figure 1B).

CX-5461 is a photosensitizer that generates ROS upon exposure to UVA

In the course of assaying pharmacogenetic interactions, we observed sporadic episodes of increased CX-5461 toxicity in wild-type animals. Increased CX-5461 toxicity was not observed when we switched from a tungsten halogen light source to a light-emitting diode light source, which generates less UVA radiation than a tungsten halogen bulb. We hypothesized that the increased toxicity was due to CX-5461-mediated photosensitivity. Photosensitivity is a common side effect of many therapeutics (Dawe and Ibbotson 2014). Clinical trials evaluating CX-5461 in patients with hematologic or advanced solid tumors have also reported cases of photosensitivity (Hilton *et al.* 2018; Khot *et al.* 2019). We used *C. elegans* as an *in vivo* model to investigate the photosensitivity of CX-5461. We focused on the effect of UVA radiation on CX-5461 for several reasons: (1) CX-5461 absorbs UVA and UVB radiation, (2) other quinolone-based molecules can trigger photosensitivity upon UVA irradiation (Dawe and Ibbotson 2014), (3) UVA passes through clouds and glass, accounting for > 90% of the UV radiation reaching the Earth's surface, and (4) UVA penetrates deep into the dermis and triggers chemical-induced photosensitivity.

First, we attempted to recreate the CX-5461-induced photosensitivity in wild-type *C. elegans*. Young adult animals were exposed to CX-5461 for ∼16 hr and then exposed to UVA radiation. Photosensitivity was measured by assessing the viability of F1 progeny from exposed animals. Wild-type

Table 1 Pharmacogenetic profiles of *C. elegans* DNA damage response mutants

Pathway	*C. elegans*	Human homolog	% viable	UVA-TMP	UVC	CPT	ETP	CX-5461
Wild-type	*N2*		100	–	–	–	–	–
Cohesin	*him-1*	*SMC1A*	84	+	++	+++	++++	+++
Chromatin remodeling	*let-418*	*CHD4*	85	+++	–	–	–	+
	hda-3	*HDAC1*	99	++	–	–	+	–
RNA binding	*gld-1*	*QKI*	88	–	–	+	–	–
DDR checkpoint	*atm-1*	*ATM*	63	++	++	+++	++	++++
	cep-1	*TP53*	99	–	++	+++	–	–
Endonuclease	*mus-81*	*MUS81*	91	++++	+++	++++	++++	++++
Helicase	*helq-1*	*HELQ*	91	–	+	++++	++	++++
	rcq-5	*RECQ5*	100	–	–	–	–	–
	rtel-1	*RTEL*	94	++	–	–	+++	+
	wrn-1	*WRN*	99	–	–	–	–	–
	smrc-1	*SMARCAL1*	71	++	++	++++	++++	++++
Translesion synthesis	*polh-1*	*POLH*	93	++++	++++	+	++	++++
	polz-1/rev-3	*REV3*	91	++++	++	–	–	++++
	polk-1	*POLK*	100	–	–	–	ND	–
Fanconi anemia	*dog-1*	*FANCJ*	98	+	–	–	+++	–
	fncm-1	*FANCM*	99	+++	+	–	–	–
	fan-1	*FAN1*	99	++++	–	–	–	–
	fcd-2	*FANCD2*	100	+	–	–	–	–
NER	*ercc-1*	*ERCC1*	66	++++	++++	–	–	++++
	xpa-1	*XPA*	92	+++	+++	–	–	+++
MMR	*msh-2*	*MSH2*	86	+++	–	+++	+	–
HDR	*brd-1*	*BARD1*	99	++	–	++++	+	++
	rfs-1	*RAD51C*	94	+++	–	++++	++	++
NHEJ	*hsr-9*	*TP53BP1*	91	–	–	–	ND	–
	cku-80	*KU80*	100	–	–	–	–	–
	lig-4	*LIG4*	99	–	–	–	–	–
MMEJ	*polq-1*	*POLQ*	99	++	–	–	+++	++

++++, 0–25%; +++, 26–50%; ++, 51–75%; +, 76–85%; -, 86–100% viability relative to untreated. TMP, trimethylpsoralen; CPT, camptothecin; ETP, etoposide; DDR, DNA damage response; NER, nucleotide excision repair; MMR, mismatch repair; HDR, homology-directed repair; NHEJ, nonhomologous end joining; MMEJ, microhomology-mediated end-joining.

animals were not sensitive to CX-5461 or UVA alone, but were sensitive to CX-5461 + UVA exposure (Figure 2A). Increasing either the concentration of CX-5461 or the amount of UVA radiation enhanced the cytotoxicity in a dose-dependent manner (Figure 2A). To assess if the photosensitivity was limited to the germline, we assayed CX-5461 photosensitivity in L1 larvae. Synchronized L1 larvae were arrested by starvation and treated with 100 μM CX-5461 for ~16 hr, followed by exposure to 300 J/m^2 UVA radiation. Photosensitivity was measured by assessing the developmental stage of the population after 96 hr. L1 wild-type animals were not sensitive to CX-5461 or UVA alone, but were sensitive to CX-5461 + UVA exposure with many animals failing to develop to the adult stage (Figure 2B). To test if CX-5461 photosensitivity was conserved in other species, we assayed UVA-mediated CX-5461 photosensitivity in mismatch repair-defective and -proficient human cancer cell lines (HCT116 and HT29, respectively) and in wild-type and homologous recombination-defective budding yeast (*Saccharomyces cerevisiae*). Both human colorectal cancer cell lines exhibited UVA-induced dose-dependent CX-5461-mediated photosensitivity (Figure 2C). Similarly, wild-type and *rad52* yeast also exhibited dose-dependent CX-5461-mediated photosensitivity (Figure 2D).

The phototoxicity of some fluoroquinolones can be attributed to the generation of reactive oxygen species (ROS) after exposure to UVA radiation (de Guidi *et al.* 2011). To determine whether CX-5461 generated ROS upon UVA radiation, we used H_2DCFDA as an intracellular fluorescent probe to measure ROS (Yoon *et al.* 2017) in CX-5461 + UVA-exposed *C. elegans*. We observed a significant dose-dependent ROS increase in worms treated with CX-5461 followed by UVA exposure (Figure 2E). Increasing UVA or CX-5461 increased the amount of ROS produced (Figure 2E). Taken together, these data suggest that CX-5461 is a photosensitizer that results in cytotoxicity due to the production of ROS.

TLS and NER mutants exacerbate CX-5461 photosensitivity

To test whether the CX-5461-induced photosensitivity was due to increased DNA damage or changes in the nature of the DNA damage, we tested select mutants in the panel of *C. elegans* DNA replication and repair mutants for increased photosensitivity. Most DNA repair mutants were no more photosensitive to CX-5461 + UVA than wild-type animals (Figure 3A). However, the translesion polymerase mutant *polz-1/rev-3* and the NER mutant *xpa-1* exhibited greater embryonic death than expected. These results are consistent with the observation that CX-5461 generates ROS after UVA exposure (Figure 2E), and TLS and NER are required for the

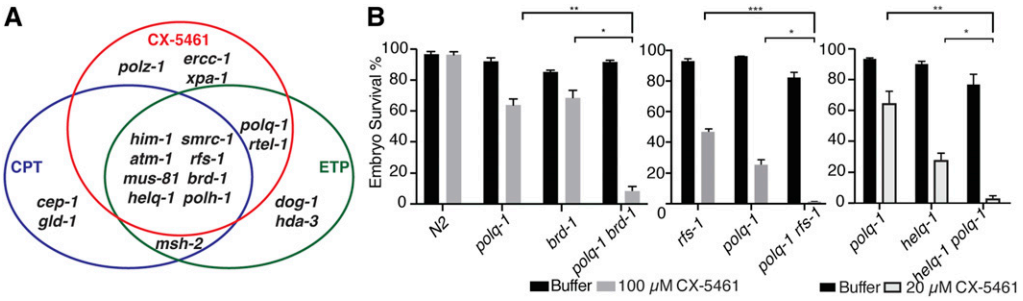

Figure 1 Genotypic sensitivity to CX-5461. (A) Genotypic sensitivity profile of CX-5461. Venn diagram shows that the CX-5461-sensitive mutants also exhibited sensitivity to other DNA-damaging agents, including the topoisomerase poisons camptothecin (CPT) and etoposide (ETP). (B) Loss of *polq-1* sensitizes homology-directed repair-associated mutants (*brd-1*, *rfs-1*, and *helq-1*) to CX-5461. The bar graph shows the embryo survival rate for adult animals treated with the indicated dose of CX-5461. Student's *t*-test: $*P < 0.05$, $**P < 0.005$, $***P < 0.0005$.

repair of DNA damage induced by ROS generated by UVA exposure (van Schendel *et al.* 2016).

CX-5461 causes transcription-blocking lesions

The NER mutant *xpa-1* was sensitive to CX-5461 and CX-5461 + UVA. NER repairs bulky single-stranded DNA lesions such as those formed by UV light and some cancer chemotherapeutics. Most NER activity is transcription-coupled. It is possible to assay the effect of DNA-damaging agents on transcription-coupled repair by exploiting the starvation-induced L1 diapause in *C. elegans*, in which replication is arrested. L1 larvae with NER defects exposed to transcription-blocking DNA-damaging agents are unable to reinitiate development when released from arrest (Astin *et al.* 2008). To test whether CX-5461 caused transcription-blocking lesions, we assayed CX-5461 + UVA sensitivity in L1-arrested NER mutants. Replication-arrested L1 larvae were exposed to CX-5461 + UVA, released from arrest, and their development stages were assessed 96 hr later. CX-5461 + UVA-treated *xpa-1* L1 larvae failed to develop to later larval stages suggesting that CX-5461 can cause transcription-blocking lesions (Figure 3B). In contrast, the replication-associated CX-5461-hypersensitive mutant *mus-81* could reinitiate development after L1 CX-5461 + UVA exposure and developed into sterile adults. These data suggest that CX-5461-induced lesions can block both transcription and replication.

CX-5461 exposure results in SNVs and GCRs

The pharmacogenetic profile of CX-5461 suggested that CX-5461 exposure caused DNA lesions that required NER or TLS for resolution, in addition to DSBs that required HDR or MMEJ for repair. To determine the frequency and spectrum of mutagenic events induced by CX-5461 and CX-5461 + UVA, we used the *eT1* genetic balancer in wild-type *C. elegans* to capture and characterize CX-5461-induced lethal mutations in the presence and absence of UVA. The *eT1* balancer is a reciprocal translocation of approximately one-half of chromosome III and one-half of chromosome V, and can capture both SNVs and copy number variations (CNVs) in balanced regions, including terminal deletion events and translocations (Rosenbluth *et al.* 1983).

Exposure to CX-5461 or CX-5461 + UVA resulted in high frequencies of strains with balanced lethal mutations and dominant sterile F1 animals, which produced no progeny (Figure 4A). Four strains with balanced recessive lethal mutations were recovered from a screen of 200 F1 progeny from individuals treated with 100 μM CX-5461. UVA radiation increased the mutagenicity of CX-5461 more than fourfold. Nineteen strains with balanced recessive lethal mutations were recovered from a screen of 200 F1 progeny from individuals treated with 100 μM CX-5461 + 100 J/m^2 of UVA radiation.

To elucidate the mutational signatures of CX-5461 and CX-5461 + UVA, we sequenced the genomes of the 23 strains with *eT1*-balanced lethal mutations. The CX-5461- and CX-5461 + UVA-treated genomes contained a range of mutation types, including large CNVs and SNVs. First, we analyzed the mutations in the balanced regions to identify the lesions responsible for the lethal phenotype. In the mutated strains, 13/23 contained large CNVs in the balanced regions that could account for the lethal phenotype (Table 2 and Figures S1–S2) and 14/23 strains contained SNVs in essential genes (Table 2).

Analysis of CX-5461-induced CNVs

Most CX-5461- and CX-5461 + UVA-treated genomes contained at least one CNV. CNVs ranged from simple deletions to complex events involving deletions, duplications, and translocations (Figures S1 and S2). The high frequency of CX-5461-induced CNVs was consistent with the observation that DNA DSB repair genes were required for CX-5461 tolerance in *C. elegans* [Table 1 and Xu *et al.* (2017)]. CNV breakpoints frequently contained regions of microhomology consistent with MMEJ (Figure 4B and Table 2). Analysis of the regions surrounding the CNV breakpoints found DNA repeats (simple, tandem, and inverted) flanking some, but not all, of the breakpoints.

Analysis of CX-5461-induced SNVs

All CX-5461-exposed genomes contained high frequencies of heterozygous and homozygous SNVs (Table 2). Genomes exposed to CX-5461 + UVA had more homozygous and

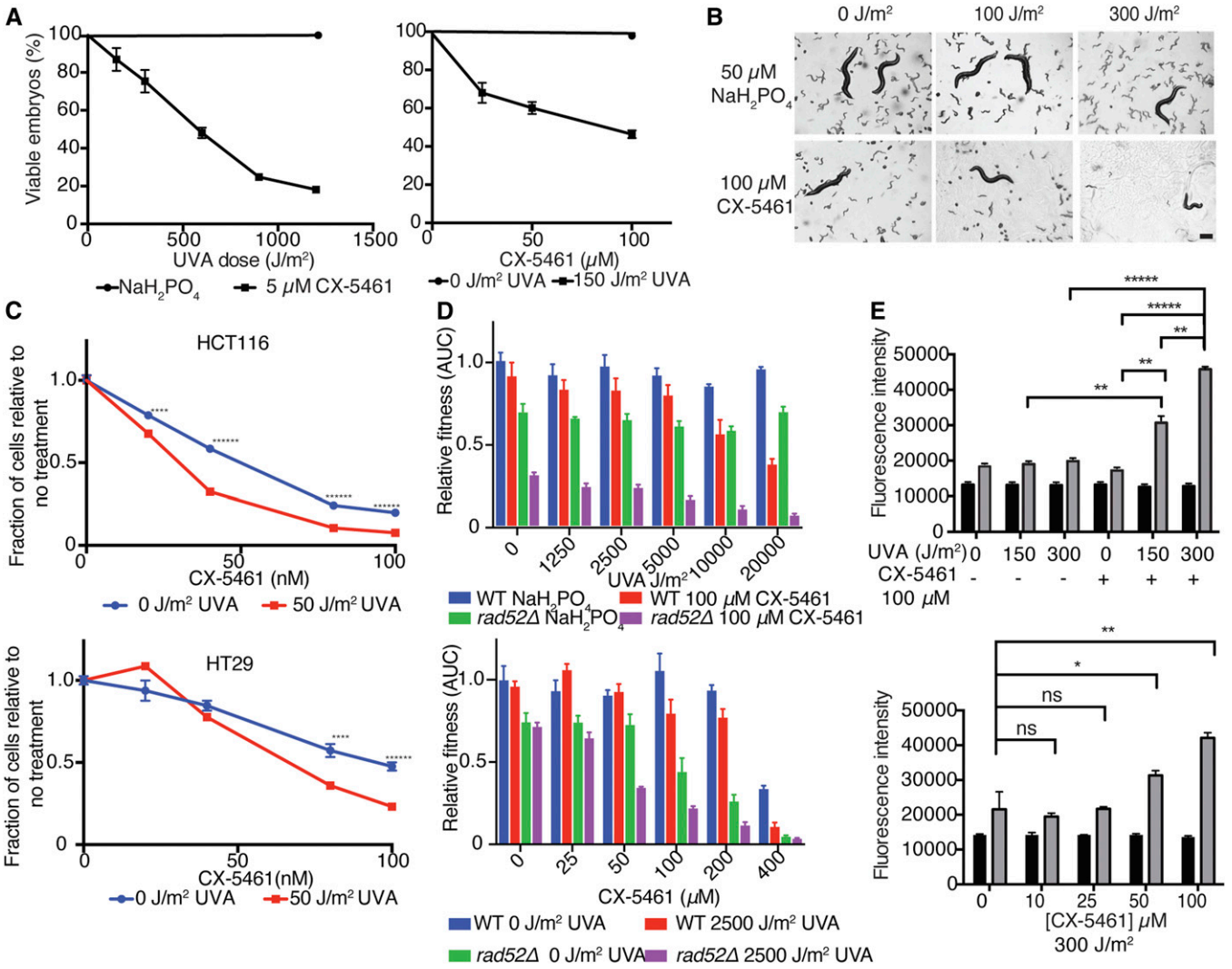

Figure 2 CX-5461 is a photosensitizer in *C. elegans*, human cancer cell lines, and yeast. (A) Viability of WT *C. elegans* embryos from adult animals exposed to CX-5461 and irradiated with UVA. Left, constant CX-5461 concentration; right, constant UVA dose. (B) Representative images of WT *C. elegans* populations 96 hr after CX-5461 + UVA exposure of synchronized WT L1 larvae. The large animals are the treated P0 individuals. Bar ~0.2 mm. (C) HCT116 and HT29 colorectal cancer cell lines were treated with increasing concentrations of CX-5461, exposed to UVA irradiation in a 96-well format, and cell nuclei counted after 96 hr. Student's *t*-test: ****$P < 0.0005$, ******$P < 0.000005$. (D) Growth curve analysis of the relative fitness of WT and *rad52*Δ yeast exposed to CX-5461 + UVA radiation. Top, fixed CX-5461 concentration; bottom, fixed UVA dose. (E) Intracellular reactive oxygen species levels in CX-5461 + UVA treated WT *C. elegans*. Top, fixed CX-5461 concentration; bottom, fixed UVA dose. Black bars: fluorescence intensity before UVA irradiation; gray bars, fluorescence intensity after UVA irradiation. Student's *t*-test *$P < 0.05$, **$P < 0.005$, *****$P < 0.000005$. AUC, area under the curve; WT, wild-type.

heterozygous SNVs compared with those exposed to CX-5461 alone (Figure 4C). The increased frequency of SNVs in the CX-5461 + UVA-treated genomes was consistent with the increased frequency of balanced lethal mutations.

All 4284 SNVs were included in the analysis because there were no obvious differences in the characteristics of the mutational profiles of heterozygous or homozygous SNVs, or between the CX-5461- and CX-5461 + UVA-induced SNVs. The SNVs were distributed throughout the genome with no bias for coding or noncoding regions (Figure 4D) or chromosome location (Figure S3 and Table S1). In total, 517 SNVs (12%) were present in 212 multinucleotide mutation (MNM) clusters consisting of 2–13 SNVs within a 1000-bp region. Of the SNVs in MNMs, > 80% were < 15 bases from the neighboring mutations (Figure 4E). It was possible that the SNVs were the product of repair or bypass of CX-5461-stabilized G4s, so we searched 100 bases 5′ and 3′ of each SNV for G4-forming structures using the QuadBase2 web server (Dhapola and Chowdhury 2016). SNVs were not strongly correlated with G4-forming sequences. Only 0.75% of mutation-flanking regions contained predicted G4s compared with 0.45% in a control set of EMS mutations from the Million Mutation Project (Thompson *et al.* 2013).

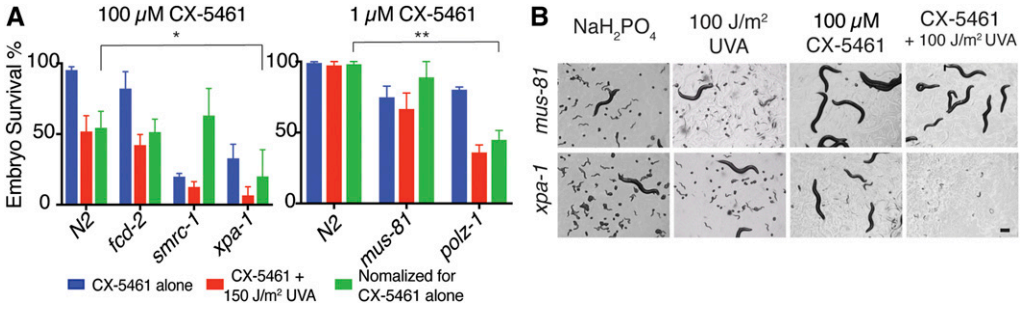

Figure 3 UVA enhances the toxicity of CX-5461. (A) Differential sensitivity of worm mutants upon exposure to CX-5461 + UVA. CX-5461-hypersensitive mutants were tested at low CX-5461 concentration (right). Note that *xpa-1* and *polz-1/rev-3* are the only mutants that are more sensitive to CX-5461 + UVA when normalized to account for the sensitivity to CX-5461 alone. Student's *t*-test: $*P < 0.05$, $**P < 0.005$. (B) Representative image showing the growth and development of worms 4 days after treatment of L1 larvae. Upon CX-5461 treatment and UVA irradiation, *mus-81* mutants developed into sterile adults, whereas *xpa-1* mutants arrested in L1. Bar, ~0.2 mm.

CX-5461-induced SNVs exhibited a distinct mutational signature. Of the SNVs, > 80% were A to X changes with nearly 50% being A to T transversions (Figure 4F). To better understand the mutagenicity of CX-5461, we used pLogo, a probability Logo generator, to examine the extended sequence context of the A to X mutations (O'Shea *et al.* 2013). We observed changes in the frequency of bases both 5′ and 3′ of the mutated adenine. Most notably, 70% of the bases immediately 3′ (+1 position) of the mutated adenine were thymine. Guanine was overrepresented in the +2 position and cytosine was overrepresented in the −1 and −2 positions. In contrast, no extended sequence context was detected flanking mutated guanine (Figure 4G). Although there was a higher frequency of SNVs in the CX-5461 + UVA samples compared with CX-5461 genomes, we saw no difference in the types of SNVs, suggesting that UVA exposure enhanced the frequency of CX-5461-induced SNVs but did not change the mutational mechanism.

To identify sequence motifs that may be more prone to CX-5461 mutagenesis, we looked for sites that were mutated in more than one line. Forty-seven sites were mutated in two or more lines (127 SNVs). We analyzed 100 bases flanking each of the frequently mutated sites for sequences predicted to form secondary structures and found that 25/47 (53%) flanking regions contained inverted or tandem repeats that were annotated in WormBase (www.wormbase.org, release WS275, 01-12-2019). For comparison, a similar analysis of 3719 regions flanking EMS-induced mutations from the Million Mutation Project (Thompson *et al.* 2013) found 753 repeats (20.2%). From this, it appears that CX-5461-induced mutations are more common in regions containing tandem or inverted repeats.

CX-5461-sensitive mutants and G4 stabilization

There are similarities between worms exposed to CX-5461 and worms lacking the *C. elegans* FANCJ ortholog *dog-1*. CX-5461 can stabilize G4s (Xu *et al.* 2017) and the loss of DOG-1 results in the formation and/or stabilization of G4 structures (Cheung *et al.* 2002). Furthermore, CX-5461-exposed animals and *dog-1* mutants exhibit large and small chromosome rearrangements, which often have MMEJ signatures at the breakpoints (Zhao *et al.* 2008; Koole *et al.* 2014). To further investigate the similarities between CX-5461 exposure and a loss of *dog-1*, we tested whether loss of *dog-1* resulted in negative genetic interactions with the CX-5461-sensitive mutants by measuring the viability of *dog-1* CX-5461-sensitive double mutants using a generational survival assay (Figure 5). The *polq-1* mutant was very sensitive to loss of DOG-1 with < 50% of the lines surviving to the third generation. *mus-81* and *brd-1* mutants were also sensitive to *dog-1*-induced G4 stabilization. However, not all CX-5461-sensitive mutants exhibited genetic interaction with *dog-1* as the loss of *polz-1/rev-3* did not affect the viability of *dog-1* mutants.

CX-5461 intercalates into DNA

The broad distribution of CX-5461-induced mutations and the CX-5461 sensitivity of TLS mutants suggested that CX-5461 can affect DNA even in the absence of G4 structures. Previous *in silico* analysis predicted that the pharmacophore of CX-5461 can intercalate into a DNA fragment (Protein Data Bank code 1Z3F) (Canals *et al.* 2005) in a manner similar to the antineoplastic agent ellipticine (Andrews *et al.* 2013). To test whether CX-5461 could intercalate into DNA, we incubated CX-5461 with a PCR-generated dsDNA and visualized the migration of DNA on a 1% agarose gel with the dsDNA-specific dye SYBR-Safe. Incubation of the dsDNA with CX-5461 resulted in a slower-migrating DNA band suggesting that intercalation had occurred (Figure 6A). The disruption of dsDNA was greater when the DNA was denatured and reannealed in the presence of CX-5461. At higher concentrations, the DNA-CX-5461 complex did not migrate into the gel (Figure 6A).

Intercalation of ellipticine into DNA results in partial unwinding and distortion of the DNA duplex (Canals *et al.* 2005). To determine whether CX-5461 intercalation distorts DNA's structure and whether G4 sequences were required, we incubated a PCR product predicted to form a G4 and a PCR product that was non-G4 with MBN, which cleaves single-stranded or distorted dsDNA, for 1 hr at the specified temperature, and assessed the endonuclease activity on a 1%

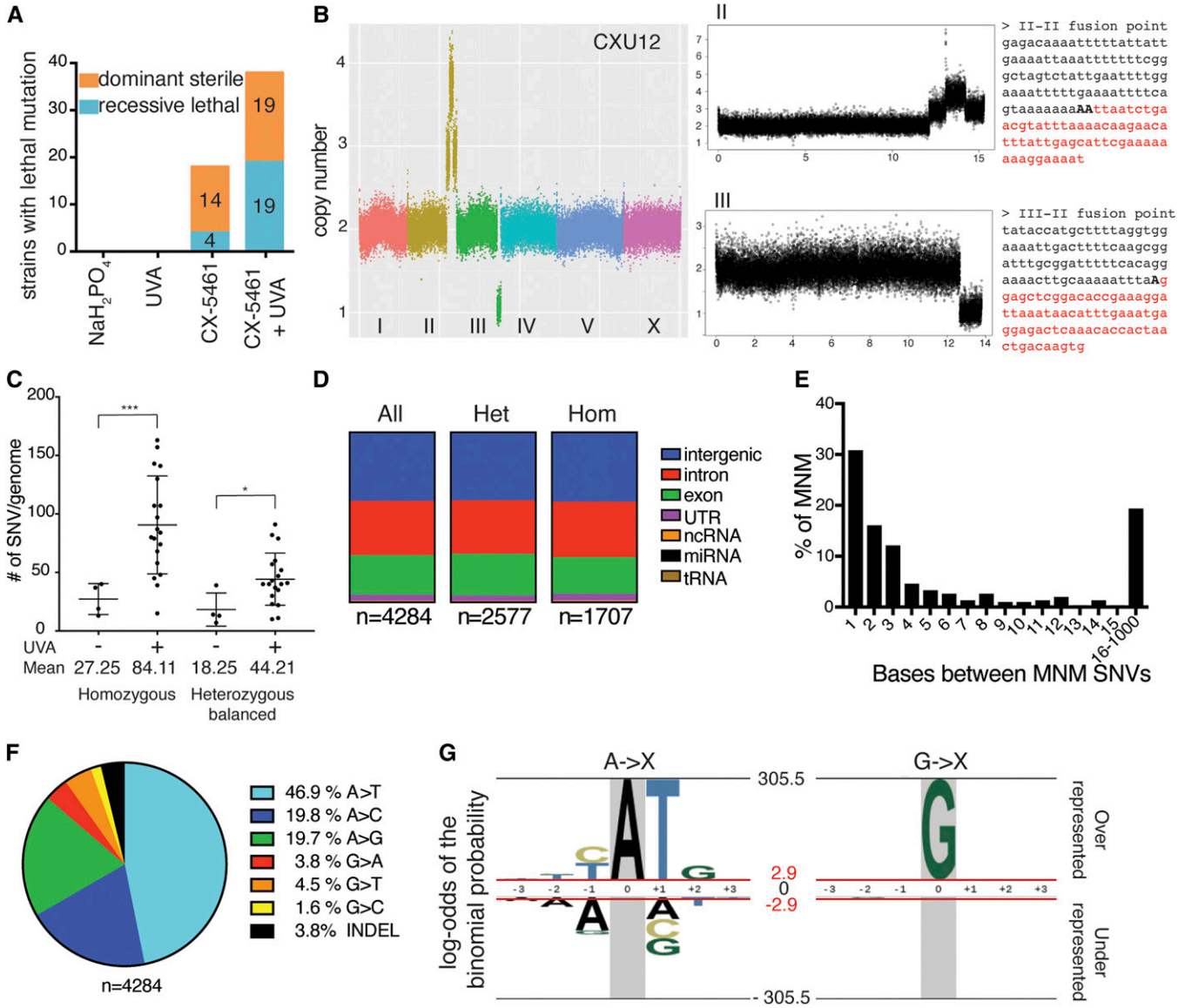

Figure 4 Exposure to CX-5461 or CX-5461 + 100 J/m^2 UVA results in high frequencies of mutations. (A) Number of balanced recessive lethal mutations and dominant sterile mutations. n = 200 for each condition. (B) Coverage plot of CX-5461 + UVA-induced genome rearrangements in sample CXU12. Whole genome (left). Detailed coverage plot of chromosome II (top right) and chromosome III (bottom right). Sequence at the fusion shown on right. Microhomology in bold. (C) Number of homozygous and heterozygous balanced SNVs/genome. Welch's t-test: ***$P < 0.0005$, *$P < 0.05$. (D) Distribution of SNVs in coding and noncoding elements. (E) Distance between SNVs in MNMs. (F) SNV mutational signature of CX-5461. (G) Probability LOGO of extended sequence context of CX-5461-induced SNVs. Het, heterozygous; Hom, homozygous; INDEL, insertion/deletion; MNM, multinucleotide mutation; SNV, single-nucleotide variation.

Syber-Safe-containing agarose gel. CX-5461 protected both G4- and non-G4-containing DNA fragments from MBN activity relative to DNA without CX-5461 (Figure 6B). At 40°, both PCR products without CX-5461 were degraded, whereas the samples containing CX-5461 were not degraded, suggesting that CX-5461 could increase the thermal stability of dsDNA. To test whether CX-5461 inhibited MBN activity directly, we increased the temperature by 10° every 5 min from 25° to 75°. At higher temperatures, MBN could degrade samples containing CX-5461, demonstrating that CX-5461 did not inhibit MBN (Figure S4).

Discussion

Key to the development of new anticancer therapeutic agents is understanding their off-target effects, mechanisms, and genotypic dependencies. While advances in target identification, chemical synthesis, and *in vitro* analysis have led to improvements in drug development, less progress has been made in improving toxicity and efficacy assays. The most common assay for mutagenicity is the bacteria-based Ames test (Mortelmans and Zeiger 2000), which has been used to assess the mutagenicity, photomutagenicity, and phototoxicity of chemotherapeutics (Wang *et al.* 2009). The efficacy of

Table 2 CX-5461-induced SNVs and CNVs

Treatment	Line	SNVs	Balanced heterozygous SNVs	Homozygous SNVs	Balanced CNVs	Putative lethal mutation
CX-5461	1	68	14	52	III del	
	2	58	5	51	V del	
	3	348	47	11		*chc-1* stop
	4	46	13	19		*F54C8.4* stop
CX-5461 + UVA	1	159	38	62		plrg-1 FS
	2	283	52	117	III del	
	3	190	34	107		*mrpl-1*
	4	241	60	130	III del	*strd-1/mlc-7*
	5	144	37	80	V del	
	6	258	57	143	III dp	Multiple
	7	178	45	87		*hpo-26*
	8	121	35	68	III del/inv	
	9	179	52	95	V del III inv	Multiple
	10	201	33	107		T05H4.10
	11	151	35	74	V dp	*npp-16*
	12	138	23	56	III del	
	13	54	11	15	V trans	
	14	485	89	157	V del	*let-413*
	15	243	43	84		*klp*-7
	16	154	22	39		*pri-1*
	17	222	39	79		ncx-2
	18	168	29	43	III del	
	19	195	10	31		None

SNV, single-nucleotide variation; CNV, copy number variations; Del, deletion; Dp, duplication; Inv, inversion; trans, translocation; FS, frameshift.

the Ames test is limited because bacteria lack many of the genes responsible for the xenobiotic metabolism of drugs and have different DNA damage repair pathways to eukaryotes, and the test only assays the reversion frequency of a single mutation. The small size, ease of handling, and powerful genetic tools of *C. elegans* provide a sophisticated *in vivo* toxicity assay that combines the technical advantages of a microorganism with greater biological complexity, and a gene complement more akin to that of humans. Furthermore, the cytochrome P450-based metabolic capabilities of *C. elegans* are broadly similar to those of mammals (Harlow *et al.* 2018). For these reasons, *C. elegans* has been used as an *in vivo* model system to predict the effect of chemicals on mammalian development (Harlow *et al.* 2016), germline function (Allard *et al.* 2013; Shin *et al.* 2019), mutagenicity (Meier *et al.* 2014), and toxicity (Gao *et al.* 2018). We have used a complementary suite of mutagenicity, mutational profiles, and genotypic sensitivity assays that utilize *C. elegans* to characterize the new anticancer chemotherapeutic CX-5461.

Some anticancer drugs, such as vemurafenib, tamoxifen, and docetaxel, and many quinolone-based drugs, can cause phototoxic reactions (Dawe and Ibbotson 2014; Ibbotson 2018). CX-5461, which contains a quinolone backbone, has resulted in photosensitivity in some patients (Hilton *et al.* 2018; Khot *et al.* 2019). We were able to phenocopy the photosensitivity in *C. elegans* and determine that the light sensitivity was accompanied by ROS-mediated phototoxicity. We demonstrate that *C. elegans* can be used as an animal model to investigate drug-associated photosensitivity and test genetic and environmental factors, affecting both photosensitivity and resistance. Given the strong ROS-mediated phototoxicity and drug properties of CX-5461, CX-5461 may be useful for photodynamic anticancer therapy, in which targeted light is used to activate a photosensitizer within cancer cells leading to cell death.

Many factors can affect the concentration of compounds in the germ cells that will give rise to the embryos that are being measured in sensitivity assays. *C. elegans* has a cuticle that is relatively impermeable to solutes; therefore, compounds must be ingested and pass through intestinal cells, the pseudocoelom, and gonadal sheath cells to reach the germ cells. *C. elegans* also has a robust xenobiotic metabolism that could also affect the effective concentration of compounds within the worm (Harlow *et al.* 2018). For these reasons, the effective drug concentrations used in *C. elegans* sensitivity assays are not predictable and therefore the concentrations used in *C. elegans* culture cannot be directly translated to effective doses in patients. *C. elegans* has proved to be an excellent model for the investigation of the mutagenicity and mutational profiles of DNA damage response mutants or genotoxic compounds (Zhao *et al.* 2008; Meier *et al.* 2014; van Schendel *et al.* 2016). CX-5461 was mutagenic and the mutagenicity was increased by exposure to UVA light. The recessive mutation frequencies for CX-5461 and CX-5461 + UVA were comparable to exposure to 5 mM and 25 mM EMS, a common alkylating mutagen, or 10 and 25 gy γ-radiation (Rosenbluth *et al.* 1983).

CX-5461-treated genomes had complex mutational profiles that included both CNVs and SNVs. The nature of CX-5461-DNA lesions can be inferred from the mutational signature and the genes required for CX-5461 tolerance. For example, it is unlikely that CX-5461 generates ICLs because

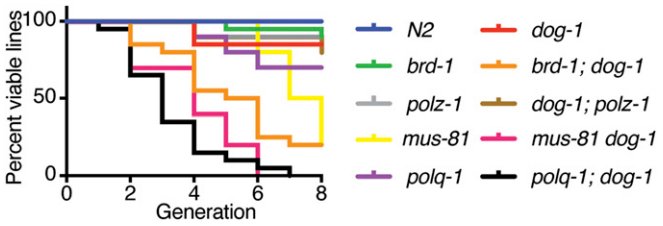

Figure 5 Effect of G-quadruplex stabilization on CX-5461-sensitive mutants. Multigenerational fitness assay. Loss of *polq-1*, *mus-81*, or *brd-1* reduced the fitness of *dog-1* mutants.

loss of the key Fanconi anemia pathway gene, *fcd-2*, did not result in CX-5461 sensitivity. CNVs are indicative of DSB formation and repair. The major pathways for the repair of CX-5461-induced DSBs in *C. elegans* appear to be MMEJ and HDR. Simultaneous loss of both pathways resulted in hypersensitivity to CX-5461. Two of the most informative CX-5461-sensitive mutants are *rfs-1* and *polq-1*. RFS-1 mediates HDR at replication fork-blocking lesions but not at IR-induced DSBs (Ward *et al.* 2007). POLQ-1 promotes MMEJ mutagenic bypass of replication fork-stalling lesions (van Schendel *et al.* 2016) and *dog-1*-induced G4s (Koole *et al.* 2014). This strongly suggests that CX-5461 does not cause DSBs directly, but rather generates replication-blocking lesions that can lead to breaks. This is further supported by the observation that *polq-1*, *rfs-1*, and other genes required for the tolerance of CX-5461, such as *brd-1*, *smrc-1*, and *xpf-1*, are also involved in the bypass or repair of replication-blocking G4 structures that form in *dog-1* mutants (Youds *et al.* 2006; Ward *et al.* 2007; Koole *et al.* 2014; Yang *et al.* 2019), and are essential for the multigenerational survival of *dog-1* mutants (Figure 5). However, we observed very few G4-forming sequences in the regions flanking SNVs or CNV breakpoints, and we demonstrated that CX-5461 can intercalate into non-G4-forming DNA sequences. Taken together, these data suggest that CX-5461 results in DNA lesions or structures that can stall or collapse replication forks, leading to DSBs even in the absence of G4s.

CX-5461 and CX-5461 + UVA exposure resulted in a high frequency of SNVs. The CX-5461 A–N mutation signature was similar to the mutational signatures observed in human cancers that have been exposed to aristolochic acid (Hoang *et al.* 2013; Poon *et al.* 2013). However, the extended-sequence context differed between CX-5461 (CATG) and aristolochic acid (T/CAG). Aristolochic acid results almost exclusively in A–T changes, whereas CX-5461 results in A–N changes. The A–T changes resulting from aristolochic acid treatment are dependent on the translesion polymerase polζ (Hashimoto *et al.* 2016). The high frequency of A–N SNVs, the presence of clustered MNMs, and the CX-5461 hypersensitivity of TLS mutants confirm that TLS is needed to bypass CX-5461-induced lesions.

How might CX-5461 trigger TLS? *In silico* analysis predicts that the pharmacophore of CX-5461 can intercalate into the DNA sequence CGATCG (Andrews *et al.* 2013) in a configuration similar to that of the antineoplastic agent ellipticine. When ellipticine intercalates into DNA, there is a slight unwinding of the ApT and a lengthening of the DNA (Canals *et al.* 2005), which could be consistent with the gel shifts we observed with DNA incubated with CX-5461. This distortion could make the ApT more prone to TLS-mediated mutagenesis either directly or through secondary reactions with the exposed adenine. Furthermore, both aristolochic acid and ellipticine can form covalent DNA adducts after reductive activation by cytochrome P450. It is possible that CX-5461 forms covalent adducts with DNA upon metabolic processing in *C. elegans*.

Overall, we found that CX-5461 shares many properties with ellipticine: both can intercalate into DNA (Andrews *et al.* 2013), induce the formation of ROS (Kim *et al.* 2011), and inhibit RNA Pol I (Drygin *et al.* 2011; Andrews *et al.* 2013). Ellipticine also inhibits topoisomerase IIα and can form covalent DNA adducts (Stiborová *et al.* 2012). Recently, it was demonstrated that the cytotoxicity of CX-5461 in cell lines is mediated, at least in part, by the inhibition of topoisomerase IIα (Bruno *et al.* 2020). These properties are consistent with the effects of CX-5461 on *C. elegans* but will require further experiments for confirmation. Ellipticine belongs to a family of promising anticancer therapeutics with a wide range of cellular effects similar to those of anthracycline-based chemotherapeutics such as doxorubicin. However, ellipticines

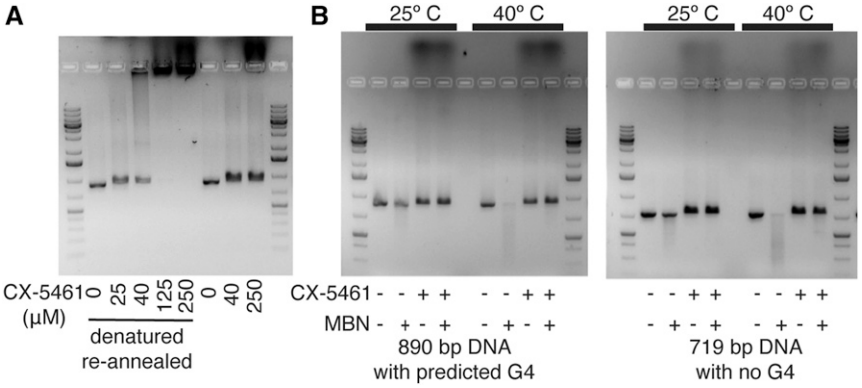

Figure 6 CX-5461 stabilizes DNA duplex structures. (A) CX-5461 binds to and impedes the migration of double-stranded DNA on a 1% agarose gel. CX-5461 binding is enhanced by DNA denaturation and reannealing (lanes 2–6). The effect was less in samples that were incubated without denaturation and reannealing (lanes 7–9). (B) CX-5461 stabilizes DNA and the complex was more resistant to mung bean nuclease (MBN) cleavage.

have failed in stage 1 or 2 clinical trials due to adverse side effects (Andrews *et al.* 2013). Based on the mechanistic similarities between ellipticine and CX-5461, it is possible that CX-5461 may elicit a response in tumor cells that is similar to that to ellipticine with fewer adverse side effects.

In summary, *C. elegans* is a powerful platform with which to interrogate the *in vivo* biological properties of both new and established anticancer therapeutic agents. The mutant panel we assembled and queried with DNA-damaging agents provides valuable information about the types of damage generated by DNA-damaging therapeutics. From these data, we have found that CX-5461 is a multimodal anticancer agent with mechanistic similarities to ellipticines and anthracyclines. This suggests that CX-5461 may be a broadly applicable anticancer drug with a therapeutic range beyond HDR-deficient tumors.

Acknowledgments

This study was funded by the Canadian Cancer Society Research Institute (grant number 702975) to PH. The authors thank members of the Stirling and Hieter labs for discussion. Some strains were provided by the CGC, which is funded by NIH Office of Research Infrastructure Programs (P40 OD010440). We thank the Moerman lab and the Million Mutation Project for the *smrc-1(gk176502)*, *smrc-1(gk784642)*, and *polz-1/rev-3(gk919715)* alleles.

Literature Cited

Allard, P., N. C. Kleinstreuer, T. B. Knudsen, and M. P. Colaiácovo, 2013 A C. elegans screening platform for the rapid assessment of chemical disruption of germline function. Environ. Health Perspect. 121: 717–724. https://doi.org/10.1289/ehp.1206301

Andrews, W. J., T. Panova, C. Normand, O. Gadal, I. G. Tikhonova *et al.*, 2013 Old drug, new target: ellipticines selectively inhibit RNA polymerase I transcription. J. Biol. Chem. 288: 4567–4582. https://doi.org/10.1074/jbc.M112.411611

Astin, J. W., N. J. O'Neil, and P. E. Kuwabara, 2008 Nucleotide excision repair and the degradation of RNA pol II by the Caenorhabditis elegans XPA and Rsp5 orthologues, RAD-3 and WWP-1. DNA Repair (Amst.) 7: 267–280. https://doi.org/10.1016/j.dnarep.2007.10.004

Barretina, J., G. Caponigro, N. Stransky, K. Venkatesan, A. A. Margolin *et al.*, 2012 The Cancer Cell Line Encyclopedia enables predictive modelling of anticancer drug sensitivity. Nature 483: 603–607 (erratum: Nature 492: 290). https://doi.org/10.1038/nature11003

Basu, A., N. E. Bodycombe, J. H. Cheah, E. V. Price, K. Liu *et al.*, 2013 An interactive resource to identify cancer genetic and lineage dependencies targeted by small molecules. Cell 154: 1151–1161. https://doi.org/10.1016/j.cell.2013.08.003

Brenner, S., 1974 The genetics of Caenorhabditis elegans. Genetics 77: 71–94.

Bruno, P. M., M. Lu, K. A. Dennis, H. Inam, C. J. Moore *et al.*, 2020 The primary mechanism of cytotoxicity of the chemotherapeutic agent CX-5461 is topoisomerase II poisoning. Proc. Natl. Acad. Sci. USA 117: 4053–4060. https://doi.org/10.1073/pnas.1921649117

Canals, A., M. Purciolas, J. Aymamí, and M. Coll, 2005 The anticancer agent ellipticine unwinds DNA by intercalative binding in an orientation parallel to base pairs. Acta Crystallogr. D Biol. Crystallogr. 61: 1009–1012. https://doi.org/10.1107/S0907444905015404

C. elegans Deletion Mutant Consortium, 2012 Large-scale screening for targeted knockouts in the Caenorhabditis elegans genome. G3 (Bethesda) 2: 1415–1425. https://doi.org/10.1534/g3.112.003830

Cheung, I., M. Schertzer, A. Rose, and P. M. Lansdorp, 2002 Disruption of dog-1 in Caenorhabditis elegans triggers deletions upstream of guanine-rich DNA. Nat. Genet. 31: 405–409. https://doi.org/10.1038/ng928

Dawe, R. S., and S. H. Ibbotson, 2014 Drug-induced photosensitivity. Dermatol. Clin. 32: 363–368. https://doi.org/10.1016/j.det.2014.03.014

de Guidi, G., G. Bracchitta, and A. Catalfo, 2011 Photosensitization reactions of fluoroquinolones and their biological consequences. Photochem. Photobiol. 87: 1214–1229. https://doi.org/10.1111/j.1751-1097.2011.00978.x

Dhapola, P., and S. Chowdhury, 2016 QuadBase2: web server for multiplexed guanine quadruplex mining and visualization. Nucleic Acids Res. 44: W277–W283. https://doi.org/10.1093/nar/gkw425

Drygin, D., A. Lin, J. Bliesath, C. B. Ho, S. E. O'Brien *et al.*, 2011 Targeting RNA polymerase I with an oral small molecule CX-5461 inhibits ribosomal RNA synthesis and solid tumor growth. Cancer Res. 71: 1418–1430. https://doi.org/10.1158/0008-5472.CAN-10-1728

Gao, S., W. Chen, Y. Zeng, H. Jing, N. Zhang *et al.*, 2018 Classification and prediction of toxicity of chemicals using an automated phenotypic profiling of Caenorhabditis elegans. BMC Pharmacol. Toxicol. 19: 18. https://doi.org/10.1186/s40360-018-0208-3

Garnett, M. J., E. J. Edelman, S. J. Heidorn, C. D. Greenman, A. Dastur *et al.*, 2012 Systematic identification of genomic markers of drug sensitivity in cancer cells. Nature 483: 570–575. https://doi.org/10.1038/nature11005

Harlow, P. H., S. J. Perry, S. Widdison, S. Daniels, E. Bondo *et al.*, 2016 The nematode Caenorhabditis elegans as a tool to predict chemical activity on mammalian development and identify mechanisms influencing toxicological outcome. Sci. Rep. 6: 22965. https://doi.org/10.1038/srep22965

Harlow, P. H., S. J. Perry, A. J. Stevens, and A. J. Flemming, 2018 Comparative metabolism of xenobiotic chemicals by cytochrome P450s in the nematode Caenorhabditis elegans. Sci. Rep. 8: 13333. https://doi.org/10.1038/s41598-018-31215-w

Hashimoto, K., R. Bonala, F. Johnson, A. P. Grollman, and M. Moriya, 2016 Y-family DNA polymerase-independent gap-filling translesion synthesis across aristolochic acid-derived adenine adducts in mouse cells. DNA Repair (Amst.) 46: 55–60. https://doi.org/10.1016/j.dnarep.2016.07.003

Hilton, J., D. W. Cescon, P. Bedard, H. Ritter, D. Tu *et al.*, 2018 CCTG IND.231: a phase 1 trial evaluating CX-5461 in patients with advanced solid tumors. Ann. Oncol. 29: iii8. https://doi.org/10.1093/annonc/mdy048.003

Hoang, M. L., C. H. Chen, V. S. Sidorenko, J. He, K. G. Dickman *et al.*, 2013 Mutational signature of aristolochic acid exposure as revealed by whole-exome sequencing. Sci. Transl. Med. 5: 197ra102. https://doi.org/10.1126/scitranslmed.3006200

Ibbotson, S., 2018 Drug and chemical induced photosensitivity from a clinical perspective. Photochem. Photobiol. Sci. 17: 1885–1903. https://doi.org/10.1039/C8PP00011E

Iorio, F., T. A. Knijnenburg, D. J. Vis, G. R. Bignell, M. P. Menden *et al.*, 2016 A landscape of pharmacogenomic interactions in cancer. Cell 166: 740–754. https://doi.org/10.1016/j.cell.2016.06.017

Itani, O. A., S. Flibotte, K. J. Dumas, D. G. Moerman, and P. J. Hu, 2016 Chromoanasynthetic genomic rearrangement identified in a N-Ethyl-N-Nitrosourea (ENU) mutagenesis screen in Caenorhabditis elegans. G3 (Bethesda) 6: 351–356. https://doi.org/10.1534/g3.115.02425

Jiang, H., J. R. Pritchard, R. T. Williams, D. A. Lauffenburger, and M. T. Hemann, 2011 A mammalian functional-genetic approach to characterizing cancer therapeutics. Nat. Chem. Biol. 7: 92–100. https://doi.org/10.1038/nchembio.503

Khot, A., N. Brajanovski, D. P. Cameron, N. Hein, K. H. Maclachlan *et al.*, 2019 First-in-human RNA polymerase I transcription inhibitor CX-5461 in patients with advanced hematologic cancers: results of a phase I dose-escalation study. Cancer Discov. 9: 1036–1049. https://doi.org/10.1158/2159-8290.CD-18-1455

Kim, J. Y., S. G. Lee, J. Y. Chung, Y. J. Kim, J. E. Park *et al.*, 2011 Ellipticine induces apoptosis in human endometrial cancer cells: the potential involvement of reactive oxygen species and mitogen-activated protein kinases. Toxicology 289: 91–102. https://doi.org/10.1016/j.tox.2011.07.014

Koole, W., R. Van Schendel, A. E. Karambelas, J. T. Van Heteren, K. L. Okihara *et al.*, 2014 A polymerase theta-dependent repair pathway suppresses extensive genomic instability at endogenous G4 DNA sites. Nat. Commun. 5: 3216. https://doi.org/10.1038/ncomms4216

Li, H., and R. Durbin, 2010 Fast and accurate long-read alignment with Burrows-Wheeler transform. Bioinformatics 26: 589–595. https://doi.org/10.1093/bioinformatics/btp698

Li, H., B. Handsaker, A. Wysoker, T. Fennell, J. Ruan *et al.*, 2009 The sequence alignment/map format and SAMtools. Bioinformatics 25: 2078–2079. https://doi.org/10.1093/bioinformatics/btp352

Li, L., Y. Li, J. Zhao, S. Fan, L. Wang *et al.*, 2016 CX-5461 induces autophagy and inhibits tumor growth via mammalian target of rapamycin-related signaling pathways in osteosarcoma. Onco. Targets Ther. 9: 5985–5997. https://doi.org/10.2147/OTT.S104513

Meier, B., S. L. Cooke, J. Weiss, A. P. Bailly, L. B. Alexandrov *et al.*, 2014 C. elegans whole-genome sequencing reveals mutational signatures related to carcinogens and DNA repair deficiency. Genome Res. 24: 1624–1636. https://doi.org/10.1101/gr.175547.114

Mortelmans, K., and E. Zeiger, 2000 The Ames Salmonella/microsome mutagenicity assay. Mutat. Res. Fundam. Mol. Mech. Mutagen. 455: 29–60. https://doi.org/10.1016/S0027-5107(00)00064-6

Negi, S. S., and P. Brown, 2015 rRNA synthesis inhibitor, CX-5461, activates ATM/ATR pathway in acute lymphoblastic leukemia, arrests cells in G2 phase and induces apoptosis. Oncotarget 6: 18094–18104. https://doi.org/10.18632/oncotarget.4093

O'Shea, J. P., M. F. Chou, S. A. Quader, J. K. Ryan, G. M. Church *et al.*, 2013 PLogo: a probabilistic approach to visualizing sequence motifs. Nat. Methods 10: 1211–1212. https://doi.org/10.1038/nmeth.2646

Poon, S. L., S.-T. Pang, J. R. McPherson, W. Yu, K. K. Huang *et al.*, 2013 Genome-wide mutational signatures of aristolochic acid and its application as a screening tool. Sci. Transl. Med. 5: 197ra101. https://doi.org/10.1126/scitranslmed.3006086

Rosenbluth, R. E., C. Cuddeford, and D. L. Baillie, 1983 Mutagenesis in Caenorhabditis elegans. I. A rapid eukaryotic mutagen test system using the reciprocal translocation, eTI(III;V). Mutat. Res. Fundam. Mol. Mech. Mutagen. 110: 39–48. https://doi.org/10.1016/0027-5107(83)90016-7

Rosenbluth, R. E., C. Cuddeford, and D. L. Baillie, 1985 Mutagenesis in Caenorhabditis elegans. II. A spectrum of mutational events induced with 1500 r of gamma-radiation. Genetics 109: 493–511.

Shin, N., L. Cuenca, R. Karthikraj, K. Kannan, and M. P. Colaiácovo, 2019 Assessing effects of germline exposure to environmental toxicants by high-throughput screening in C. elegans. *PLoS Genet.* 15: e1007975. https://doi.org/10.1371/journal.pgen.100797

Srivas, R., J. P. Shen, C. C. Yang, S. M. Sun, J. Li *et al.*, 2016 A network of conserved synthetic lethal interactions for exploration of precision cancer therapy. Mol. Cell 63: 514–525. https://doi.org/10.1016/j.molcel.2016.06.022

Stiborová, M., J. Poljaková, E. Martínková, J. Ulrichová, V. Šimánek *et al.*, 2012 Ellipticine oxidation and DNA adduct formation in human hepatocytes is catalyzed by human cytochromes P450 and enhanced by cytochrome b5. Toxicology 302: 233–241. https://doi.org/10.1016/j.tox.2012.08.004

Thompson, O., M. Edgley, P. Strasbourger, S. Flibotte, B. Ewing *et al.*, 2013 The million mutation project: a new approach to genetics in Caenorhabditis elegans. Genome Res. 23: 1749–1762. https://doi.org/10.1101/gr.157651.113

van Schendel, R., J. van Heteren, R. Welten, and M. Tijsterman, 2016 Genomic scars generated by polymerase theta reveal the versatile mechanism of alternative end-joining. PLoS Genet. 12: e1006368. https://doi.org/10.1371/journal.pgen.1006368

Wang, S., L. Wang, J. J. Yin, Z. Wang, P. P. Fu *et al.*, 2009 Light-induced toxic effects of tamoxifen: a chemotherapeutic and chemopreventive agent. J. Photochem. Photobiol. Chem. 201: 50–56. https://doi.org/10.1016/j.jphotochem.2008.09.013

Ward, J. D., L. J. Barber, M. I. R. Petalcorin, J. Yanowitz, and S. J. Boulton, 2007 Replication blocking lesions present a unique substrate for homologous recombination. EMBO J. 26: 3384–3396. https://doi.org/10.1038/sj.emboj.7601766

Xu, H., M. Di Antonio, S. McKinney, V. Mathew, B. Ho *et al.*, 2017 CX-5461 is a DNA G-quadruplex stabilizer with selective lethality in BRCA1/2 deficient tumours. Nat. Commun. 8: 14432. https://doi.org/10.1038/ncomms14432

Yang, B., X. Xu, L. Russell, M. T. Sullenberger, J. L. Yanowitz *et al.*, 2019 A DNA repair protein and histone methyltransferase interact to promote genome stability in the Caenorhabditis elegans germ line. *PLoS Genet.* 15: e1007992. https://doi.org/10.1371/journal.pgen.1007992

Yoon, D. S., Y. Choi, D. S. Cha, P. Zhang, S. M. Choi *et al.*, 2017 Triclosan disrupts SKN-1/Nrf2-mediated oxidative stress response in C. elegans and human mesenchymal stem cells. Sci. Rep. 7: 12592. https://doi.org/10.1038/s41598-017-12719-3

Youds, J. L., N. J. O'Neil, and A. M. Rose, 2006 Homologous recombination is required for genome stability in the absence of DOG-1 in Caenorhabditis elegans. Genetics 173: 697–708. https://doi.org/10.1534/genetics.106.056879

Zhao, Y., M. Tarailo-Graovac, N. J. O'Neil, and A. M. Rose, 2008 Spectrum of mutational events in the absence of DOG-1/FANCJ in Caenorhabditis elegans. DNA Repair (Amst.) 7: 1846–1854. https://doi.org/10.1016/j.dnarep.2008.07.011

Communicating editor: J. Nickoloff